Color modulation of electrochromic nanosheet-structured nickel-cobalt oxide thin films

Kyung Ho Kim*, Misaki Morohoshi, Yoshio Abe

School of Earth, Energy and Environmental Engineering, Kitami Institute of Technology, 165 Koen-cho, Kitami, Hokkaido 090-8507, Japan

ABSTRACT

Nickel-cobalt (Ni-Co) oxide thin films were directly grown on the fluorine-doped tin oxide (FTO)-coated glass substrates via a simple one-pot solution process using various ratios of Ni and Co precursors. All the Ni-Co oxide samples were composed of nanosheet structures that were vertically aligned on the surface of the substrates. The nanosheets of the Ni10-Co0, Ni8-Co2, Ni6-Co4, and Ni4-Co6 oxide samples uniformly covered the surface, whereas those of the Ni2-Co8 and Ni0-Co10 oxide samples were sparsely distributed. As the ratio of Co to Ni was increased, the width of the nanosheets gradually

increased. Cyclic voltammetry (CV) at a scan rate of 50 mV/s showed that the Ni8-Co2 and Ni6-Co4 oxide samples exhibited better electrochemical performance than the other oxide samples. Furthermore, all Ni-Co oxide samples except Ni0-Co10 exhibited a reversibly sustainable *in-situ* transmittance change with cycling (1000 cycles, 30000 s) and a relatively fast switching time of less than 4 s for the colored and bleached states. Herein, the color modulation from transparent to black nanosheet-structured Ni-Co oxide samples was effectively tuned by adjusting the ratios of the Ni and Co precursors.

Keywords

Nickel; Cobalt; Oxide; Nanosheet; Electrochromic; Color modulation

*Corresponding author. Kyung Ho Kim (K.H. Kim)

E-mail address: khkim@mail.kitami-it.ac.jp

1. Introduction

The requirement for electrochemically stable electrochromic films with large optical modulation and fast switching times has increased, making them a key factor in energy-saving and color-tuning applications [1-4]. Several studies have reported the electrochromic performance of inorganic metal oxides (nickel oxide (NiO) and cobalt oxide (Co_3O_4)) prepared via dry or wet chemical methods [5-9]. The optical modulation of NiO thin films prepared via reactive radio-frequency magnetron sputtering method was improved by continuously varying the crystallinity by gradually controlling the deposition temperature (25–350 ºC) [5]. Chen reported that the electrochromic performance of porous NiO nanowall thin films prepared via hydrothermal synthesis was dependent on the annealing temperature (300–400 ºC) [6]. A lower annealing temperature allowed for the higher electrochemical reaction activity of NiO. Xia reported that porous nanoflake intercrossing net-like structured Co_3O_4 thin films had noticeable electrochromism with reversible color changes from pale yellow to dark grey [7]. Firat reported that the color contrast of a Cu-doped NiO thin film comprising a uniform nanograin and smooth surface was higher than that of undoped NiO [8]. In our previous study, we investigated the electrochromic performance of nanosheet-structured NiO thin films incorporating Co and Zn dopants via a cost-effective one-pot solution method [9].

With the addition of Co dopant, the nanosheet-structured Co-doped NiO thin film exhibited higher transmittance modulation than the undoped NiO sample. Meanwhile, the morphologies of NiO changed to loose-packed nanosheet-structures with the addition of Zn dopant, consequently leading to the formation of a relatively transparent thin film. Herein, further study is needed on the morphological properties and optical modulation of electrochromic mixed metal oxide samples.

In this study, we report the electrochromic performance and morphological evolution of porous nanosheet-structured Ni-Co oxide thin films prepared via a simple solution method. Well-controlled nanosheet-structured oxide thin films have been focused on for their enhanced electrochromic performance. Furthermore, the study of the morphological properties of nanostructured Ni-Co oxide samples with a large surface area could be applied to electrochemical energy-storage devices [10-13].

2. Experimental

The Ni-Co oxide thin films were prepared by immersing the fluorine-doped tin oxide (FTO)-coated glass substrate in an aqueous solution of nickel acetate tetrahydrate ($Ni(CH_3COO)_2 \cdot 4H_2O$, 0, 2, 4, 6, 8, 10 mM), cobalt nitrate hexahydrate ($Co(NO_3)_2 \cdot 6H_2O$, 0, 2, 4, 6, 8, 10 mM), and hexamethylenetetramine ($C_6H_{12}N_4$, 10 mM) at room

temperature. With the variation in the ratio of Ni and Co precursors, the samples were indexed as Ni10-Co0, Ni8-Co2, Ni6-Co4, Ni4-Co6. Ni2-Co8, and Ni0-Co10. Using a simple and facile one-pot solution method at a growth temperature of 90 ºC for 1.5 ~ 6 h, the nanostructured samples were thoroughly rinsing with Milli-Q water and dried at 90 ºC for 24 h, followed by annealing at 300 ºC for 1 h in air. It was a relatively simple and cost-effective process for preparing nanostructured Ni-Co oxide samples compared with those in other reports [12,13].

The crystalline structure and phase were characterized using X-ray diffraction (XRD, ULTMA IV) and Fourier-transform infrared (FTIR, JASCO, FT/IR-6100). The morphology of the nanostructures was characterized using field-emission scanning electron microscopy (FESEM, JSM-6701F). The elemental composition was analyzed using energy-dispersive X-ray spectroscopy (EDS, JSM-6510A). Cyclic voltammetry (CV, HSV-100, HOKUTO DENKO) was performed using a typical three-electrode system with a Ni-Co oxide sample as the working electrode, Pt as the counter electrode, and Ag/AgCl as the reference electrode in a 1 M KOH as the electrolyte [14]. Air and a quartz glass cell filled with 1 M KOH were used as references for the *in-situ* transmittance.

3. Results and discussion

Figure 1 shows the FESEM images of the Ni-Co oxide samples with various Ni and Co precursors ratios. All the Ni-Co oxide samples have the nanosheet structures that were vertically aligned on the surface of FTO substrates. As shown in Fig.S1(a) (Supplementary Information), only the diffraction peaks related to the FTO substrate are observed (JCPDS No.41-1445). From the FTIR spectra (Fig.S1(b)), without annealing treatment, there are non-hydrogen bonded OH groups at ~3650 cm^{-1} and metal-OH bending vibration at ~500 cm^{-1}, which indicate a hydroxide phase [13,15,16]. After annealing at 300 ºC, these absorption peaks disappear, and a metal-oxygen (M-O) stretching vibration at ~400 cm^{-1} is observed [13,15,16]. These results indicate that the obtained nanostructure samples annealed at 300 ºC were amorphous phase oxide. As shown in the photographs (Fig.S2), the Ni8-Co2 and Ni2-Co8 oxide samples were yellow-like and relatively transparent, respectively. Changing the Ni-to-Co ratio enabled the effective tuning of the color of the Ni-Co oxide samples.

As shown in the top FESEM images (Fig.1(a,b)), the interconnected nanosheets of the Ni10-Co0 oxide sample are uniformly covered on the surface, and the width of the individual nanosheets is approximately 20 nm. The Ni8-Co2 (Fig.1(c), Fig.S3) and Ni6-Co4 (Fig.1(d), Fig.S3) oxide samples show highly porous morphological features, which is similar to that of the Ni10-Co0 oxide sample. The interconnected nanosheet structures

of the Ni8-Co2 and Ni6-Co4 oxide samples were uniformly distributed on the surface. With a further increase in the Co ratio (Ni4-Co6 (Fig.1(e,f)), Ni2-Co8 (Fig.1(g,h)), Ni0-Co10 (Fig.1(i), Fig.S3)), the width of the individual nanosheets gradually increases to approximately 100 nm. The Ni2-Co8 (Fig.1(g,h)) and Ni0-Co10 (Fig.1(i), Fig.S3) oxide samples show that nanosheet structures are sparsely observed on the surface. Then, bare FTO nanoparticles, hundreds of nanometers in size, were exposed on the surface (Fig.1(i), Fig.S3).

Figure 2 shows the film thickness of each Ni-Co oxide samples estimated from the cross-sectional FESEM images with different growth times. At 1.5 h of growth (Fig.S4), the Ni10-Co0, Ni8-Co2, Ni6-Co4, and Ni4-Co6 oxide samples have nanosheets uniformly covering the surface, leading to the formation of a continuous thin-film structure. However, nanosheets of the Ni2-Co8 and Ni0-Co10 oxide samples were sparsely formed, resulting in a discontinuous structure. Our previous study reported that the nanosheet structures of nickel hydroxide ($Ni(OH)_2$) were randomly formed on the surface of FTO during the initial growth and uniformly covered with increasing growth time [9]. In contrast, cobalt hydroxide ($Co(OH)_2$) showed morphological evolution from a compact nanowire-net structure to a spare nanosheet structure with increasing growth times [17]. At 6 h of growth, the estimated film thickness of Ni10-Co0, Ni8-Co2, Ni6-

Co4, and Ni4-Co6 are ~0.9, ~1.4, ~1.2, and ~0.6 μm, respectively. The vertical length of individual nanosheet of Ni2-Co8 and Ni0-Co10 is ~0.7 and ~1.1 μm, respectively. With increasing growth time, the vertical growth of the Ni8-Co2 and Ni6-Co4 oxide samples are faster than that of the Ni10-Co0 oxide sample. The Ni4-Co6 oxide sample exhibited relatively slow growth compared with the other samples. Notably, the length, width, and density of the nanosheet structures are strongly dependent on process factors, such as growth time, temperature, and dopants [9,17,18]. Furthermore, the Ni-Co oxide nanostructured samples are potential candidates for sustainable applications such as glucose sensor, supercapacitor, and catalytic water splitting owing to their large surface area, leading to a short ion diffusion path [12,13,19,20].

EDS elemental mapping images and spectrum of the Ni8-Co2 oxide sample are shown in Fig.3. Pt was used as the coating material, and Sn from the FTO substrate was detected in the spectrum. Ni, Co, and O are uniformly distributed on the surface. Detailed amounts are listed in Table S1, and the corresponding EDS spectra were shown in Fig.S5.

The optical transmittance modulation of the electrochromic thin films was dependent on the CV measurement conditions, that is, the scan rate, potential range, and electrolyte [2,9,21,22]. As the scan rate increases, there may not be sufficient time for ions to diffuse from the electrolyte to the nanostructures, leading to a reduced number of ions provided

in the electrochemical reaction [23]. It has been reported that the porous nanostructure with large reaction surfaces and inner spaces can be more favorable for electrochemical reactions than compact nanostructures [24,25]. In here, the electrochromic performance was characterized at a moderately high scan rate without pre-activating cycling.

Figure 4(a-f) shows the *in-situ* transmittance variation measured at a wavelength of 600 nm, applied potential between –0.20 and +0.55 V at a scan rate of 50 mV/s with cycling. At the 1000th cycle (30000 s), the transmittance variation (ΔT) of the Ni-Co oxide samples was listed in the Table 1. The obtained ΔT of the Ni10-Co0 oxide sample is ~38%, which is better than that of a similar nanostructured NiO thin film (13% @ λ = 630 nm) [26]. Meanwhile, the Ni0-Co10 oxide sample exhibited no noticeable transmittance variation during cycling (Fig.4(f)). The Ni8-Co2 oxide sample has a higher transmittance moderation than the other oxide samples (Fig.4(b)). As shown in Fig.S6, the obtained ΔT values of the Ni8-Co2 oxide sample at the 10th, 200th, 400th, and 1000th cycles were ~25, ~41, ~47, and ~49%, respectively. After the 400th cycle, the change in ΔT is moderately small and sustained. At the 1000th cycle (30000 s), the calculated optical densities (ΔOD) of the Ni10-Co0, Ni8-Co2, Ni6-Co4, Ni4-Co6, and Ni2-Co8 oxide samples are 0.39, 0.93, 0.76, 018, and 0.06, respectively.

Figure 4(g,h) shows the CV curves at a scan rate of 50 mV/s and the calculated charge

density at the 1000th cycle. All the samples had one pair of redox peaks (Fig.4(g)). The coloration and bleaching processes were associated with the oxidation and reduction peaks, respectively, which could be attributed to the following electrochemical reactions [2,5,26]:

$$Ni(OH)_2\ (bleached) + OH^- \leftrightarrow NiOOH\ (colored) + H_2O + e^- \quad [1]$$

$$Co(OH)_2\ (bleached) + OH^- \leftrightarrow CoOOH\ (colored) + H_2O + e^- \quad [2]$$

Both the current density of these redox peaks and the charge density increased in the order of Ni0-Co10, Ni2-Co8, Ni4-Co6, Ni10-Co0, Ni8-Co2, and Ni6-Co4. The ratio of the inserted and extracted charge densities of all the Ni-Co oxide samples was approximately 1 (Fig.4(h)). The Ni8-Co2 and Ni6-Co4 oxide samples distinctly exhibited superior electrochemical activities to the other oxide samples. Meanwhile, Ni0-Co10 exhibited a lower current density but was noticeably stable with cycling (Fig.S7). As listed in Table 1, the Ni8-Co2 oxide sample had a higher color efficiency (CE, ~41.1 cm^2/C) than the other samples.

Figure 5 (a,b) show the *in-situ* transmittance variation measured at a wavelength of 600 nm, applied potential of +0.55 V for 18 s (colored state) and –0.20 V for 18 s (bleached state). The calculated optical switching time of all the Ni-Co oxide samples are listed in Table 1. The Ni8-Co2 and Ni6-Co4 samples had 3-4 s for the colored state and

2-3 s for the bleached state, which are slightly slower than those of the Ni10-Co0, Ni4-Co6, and Ni2-Co8 samples (< 2 s for colored and bleached states). However, it has a fast switching time compared with other reported compact nanoparticle-structured oxides (15~20 s for colored and bleached states) [27]. This might be because the nanosheet-structured Ni-Co oxide samples provide facile ions-diffusion pathways [27,28]. The *in-situ* transmittance spectra and corresponding photographs of the Ni-Co oxide samples in the colored and bleached states are shown in Fig.5(c-e). The color of Ni10-Co0 changed from pale grey to dark brown, whereas that of Ni8-Co2 was pale yellow and black. In the colored state, the Ni8-Co2 and Ni6-Co4 samples had lower average transmittance in the visible region than other samples. In both the colored and bleached states, the Ni2-Co8 sample was highly transparent compared with the other samples. Meanwhile, there was no noticeable difference between the colored and bleached states of the Ni0-Co10 sample.

Figure 6 shows the memory test in the colored state performed for 3000 s under open-circuit condition. The transmittance degradation of the Ni10-Co0 sample (~10%) was higher than those of the other samples (< ~3%). However, all Ni-Co oxide samples exhibited excellently sustainable coloration durability, which is important for practical applications. Furthermore, no thin film detachment from the substrate was observed during cycling, and the nanosheet-structured Ni-Co oxide sample exhibited outstanding

structural stability after the electrochromic performance tests (Fig.S8).

4. Conclusions

We investigated the morphological evolution of the Ni-Co oxide samples directly grown on FTO/glass substrates via a simple and cost-effective one-pot solution method with various ratios of Ni and Co precursors. The Ni10-Co0, Ni8-Co2, Ni6-Co4, and Ni4-Co6 oxide samples had vertically aligned nanosheets on the surface of the FTO substrate, forming a continuous thin film structure. Meanwhile, the Ni2-Co8 and Ni0-Co10 oxide samples only had randomly distributed nanosheets on the surface. The width of the individual nanosheets increased with increasing Co-to-Ni ratio. The variations in the *in-situ* transmittance and CE of the Ni8-Co2 oxide sample were higher than those of the other samples. Whereas, the Ni0-Co10 oxide sample exhibited no significant transmittance change, but it exhibited excellent electrochemical stability. In the colored state, the colors of the Ni-Co oxide samples were changed from transparent to black with a moderately fast switching time. The porous and vertically well-aligned nanosheet structures of the Ni-Co oxide samples provided the advantages of electrochromic performance with large optical modulation and fast switching time.

Acknowledgments

This study was partially supported by a Grant-in-Aid for Scientific Research (C) (No. 21K04149) from the Japan Society for the Promotion of Science. The authors would like to thank Mr. Susumu Tokuda of the Open Facility Center of the Kitami Institute of Technology for technical assistance with FESEM and EDS measurements.

References

[1] W. Zhang, H. Li, E. Hopmann, A.Y. Elezzabi, Nanophotonics (2020) https://doi.org/10.1515/nanoph-2020-0474

[2] Y-H. Lee, J.S. Kang, J-H. Park, J. Kang, I-R. Jo, Y-E. Sung, K-S. Ahn, Nano Energy (2020) https://doi.org/10.1016/j.nanoen.2020.104720

[3] M. Morales-Luna, M.A. Arvizu, C.G. Granqvist, G.A. Niklasson, Thin Solid Films (2016) https://doi.org/10.1016/j.tsf.2016.06.058.

[4] B.A. Korgel, Nature (2013) https://doi.org/10.1038/500278a

[5] S. Hou, A.I. Gavrilyuk, J. Zhao, H. Geng, N. Li, C. Hua, K. Zhang, Y. Li, Appl. Surf. Sci. (2018) https://doi.org/10.1016/j.apsusc.2018.04.206

[6] Z. Chen, A. Xiao, Y. Chen, C. ZuO, S. Zhou, L. Li, J. Phys. Chem. Solids (2013) https://doi.org/10.1016/j.jpcs.2013.05.015

[7] X.H. Xia, J.P. Tu, J. Zhang, X.H. Huang, X.L. Wang, W.K. Zhang, H. Huang, Electrochem. Commun. (2008) https://doi.org/10.1016/j.elecom.2008.09.025

[8] Y.E. Firat, A. Peksoz, Electrochim. Acta (2019) https://doi.org/10.1016/j.electacta.2018.10.166

[9] K.H. Kim, Y. Ishita, Y. Abe, Mater. Lett. (2021) https://doi.org/10.1016/j.matlet.2021.130755

[10] B. Vidhyadharan, N. K.M. Zain, I.I. Misnon, R.A. Azia, J. Ismail, M.M. Yusoff, R. Jose, J. Alloys Compd. (2014) https://doi.org/10.1016/j.jallcom.2014.04.211

[11] H. Xiao, F. Qu, X. Wu, Appl. Surf. Sci. (2016) https://doi.org/10.1016/j.apsusc.2015.10.171

[12] S. Dang, Z. Wang, W. Jia, Y. Cao, J. Zhang, Mater. Res. Bull. (2019) https://doi.org/10.1016/j.materresbull.2019.04.023

[13] Y. Tang, Y. Liu, S. Yu, W. Guo, S. Mu, H. Wang, Y. Zhao, L. Hou, Y. Fan, F. Gao, Electrochim. Acta (2015) https://doi.org/10.1016/j.electacta.2015.02.095

[14] Y. Yokoiwa, Y. Abe, M. Kawamura, K.H. Kim, T. Kiba, Jap. J. Appl. Phys. 58, 055501 (2019)

[15] T.N. Ramesh, P. Vishnu Kamath, J. Power Sources (2006) https://doi.org/10.1016/j.jpowsour.2005.05.050

[16] L. Xie, Z. Hu, C. Lv, G. Sun, J. Wang, Y. Li, H. He, J. Wang, K. Li, Electrochim. Acta (2012) https://doi.org/10.1016/j.electacta.2012.05.145

[17] K.H. Kim, S. Motoyama, M. Ohara, Y. Abe, M. Kawamura, T. Kiba, Mater. Lett. (2019) https://doi.org/10.1016/j.matlet.2019.03.061

[18] K.H. Kim, S. Motoyama, Y. Abe, M. Kawamura, T. Kiba, J. Electron. Mater. (2019) https://doi.org/10.1007/s11664-019-07051-7

[19] M. Hussain, Z.H. Ibupoto, M.A. Abbasi, X. Liu, O. Nur, M. Willander, Sensor (2014) https://doi.org/10.3390/s140305415

[20] B. Abdolahi, M.B. Gholivand, M. Shamsipur, M. Amiri, Int. J. Energy Res. (2021) https://doi.org/10.1002/er.6618

[21] M.D. Rocha, B. Dunn, A. Rougier, Sol. Energy Mater. Sol. Cells (2019) https://doi.org/10.1016/j.solmat.2019.110114

[22] Q. Liu, G. Dong, Y. Xiao, M-P. Delplancke-Ogletree, F. Reniers, X. Diao, Sol. Energy Mater. Sol. Cells (2016) https://doi.org/10.1016/j.solmat.2016.07.022

[23] H. Zhang, M. Zhang, Mater. Chem. Phys. (2008) https://doi.org/10.1016/j.matchemphys.2007.10.005

[24] X.H. Xia, J.P. Tu, J. Zhang, X.L. Wang, W.K. Zhang, H. Huang, Electrochem. Acta (2008) https://doi.org/10.1016/j.electacta.2008.03.047

[25] X.H. Xia, J. Zhang, X.L. Wang, W.K. Zhang, H. Huang, Sol. Energy Mater. Sol. Cells (2008) https://doi.org/10.1016/j.solmat.2008.01.009

[26] D.S. Dalavi, M.J. Suryavanshi, D.S. Patil, S.S. Mali, A.V. Moholkar, S.S. Kalagi, S.A. Vanalkar, S.R. Kang, J.H. Kim, P.S. Patil, Appl. Surf. Sci. (2011) https://doi.org/10.1016/j.apsusc.2010.10.037

[27] A. Martinez-Luevanos, J. Oliva, C.R. Garcis, F. Avalos-Belmontes, M.A. Garcia-

Lobato, Appl. Phys. A (2017) https://doi.org/10.1016/j.mset.2020.06.008

[28] N. Hu, Z. Tang, P.K. Shen, RSC Adv. (2018) https://doi.org/10.1039/c8ra03599g

Table 1. The *in-situ* transmittance at the bleached ($T_{bleached}$) and colored ($T_{colored}$), ΔT at 1000th CV cycle, CE, and switching time for bleached (t_b) and colored (t_c) states.

	$T_{bleached}$ (%)	$T_{colored}$ (%)	ΔT (%)	*CE* (cm^2/C)	t_b (s)	t_c (s)
Ni10-Co0	~63	~25	~38	~38.1	~0.5	~1.5
Ni8-Co2	~56	~7	~49	~41.1	~2.5	~4.0
Ni6-Co4	~35	~6	~29	~29.7	~2.0	~3.5
Ni4-Co6	~71	~48	~23	~25.2	~0.5	~1.0
Ni2-Co8	~75	~65	~10	~21.2	~0.5	~1.0
Ni0-Co10	–	–	–	–	–	–

Figure captions

Fig.1. FESEM images of Ni-Co oxide samples directly prepared on FTO/glass substrates; (b,f,h) high magnified images marked by dotted regions in (a,e,g); Scale bar in inset figure (a,c,d,e,g,i) was 1 μm; Growth time was 6 h.

Fig.2. Film thickness of Ni-Co oxide samples with growth times.

Fig.3. Electron image (a), EDS elemental maps (b-d), and spectrum (e) of Ni8-Co2 oxide sample; Ni (b), Co (c), O (d).

Fig.4. The *in-situ* transmittance variation at a wavelength of 600 nm with cycling (a-f), CV curves (g), and charge density (h) of Ni-Co oxide samples.

Fig.5. The *in-situ* transmittance variation at a wavelength of 600 nm with time (a,b), *in-situ* transmittance spectra (c,d), and photographs (e) of Ni-Co oxide samples under applied potential of +0.55V (colored state) and –0.20 V (bleached state) during 18 s for each; Dotted lines were guide for eye.

Fig.6. The *In-situ* transmittance variation at a wavelength of 600 nm as a function of memory time.

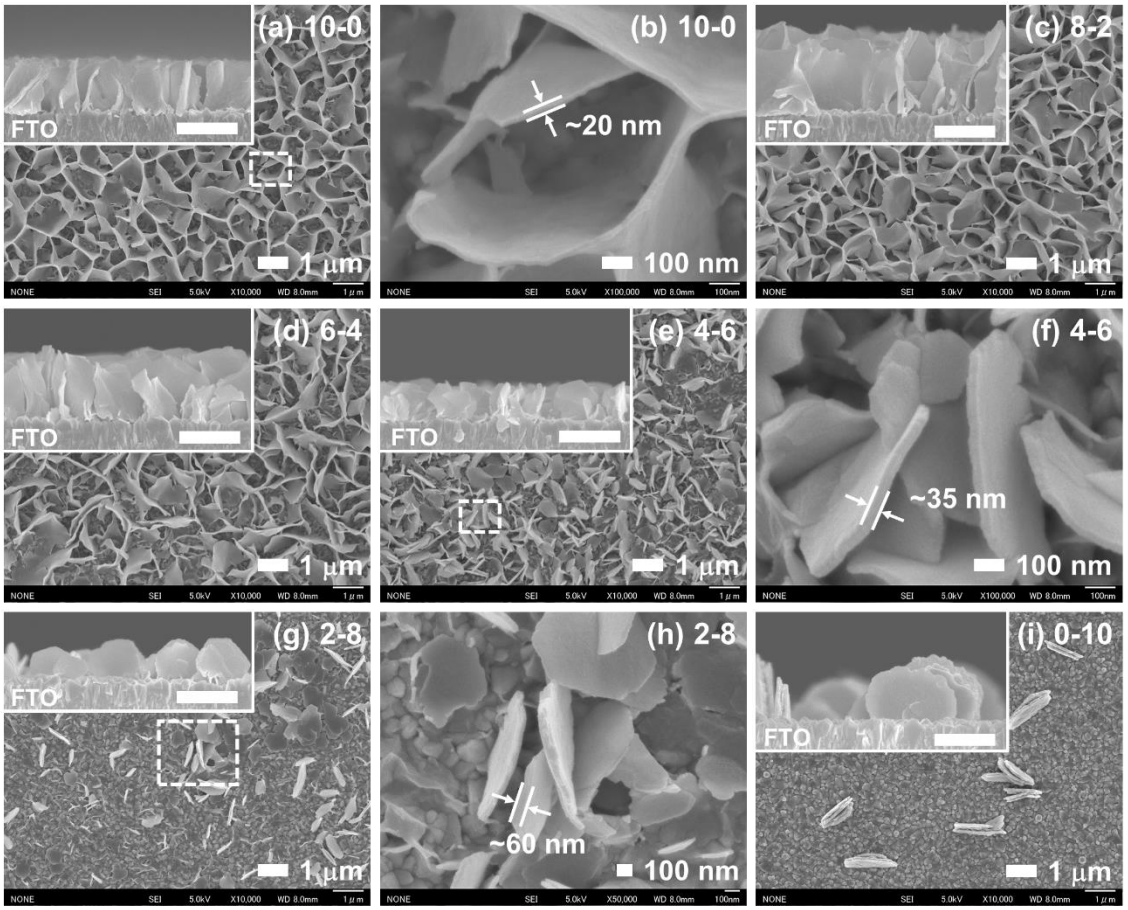
(a) 10-0
FTO
1 μm
(b) 10-0
~20 nm
100 nm
(c) 8-2
FTO
1 μm
(d) 6-4
FTO
1 μm
(e) 4-6
FTO
1 μm
(f) 4-6
~35 nm
100 nm
(g) 2-8
FTO
1 μm
(h) 2-8
~60 nm
100 nm
(i) 0-10
FTO
1 μm

Fig.1.

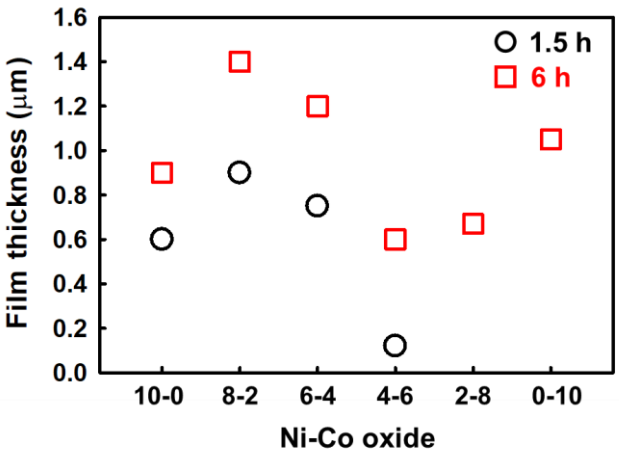
Film thickness (μm)
1.6
1.4
1.2
1.0
0.8
0.6
0.4
0.2
0.0
1.5 h
6 h
10-0
8-2
6-4
4-6
2-8
0-10
Ni-Co oxide

Fig.2.

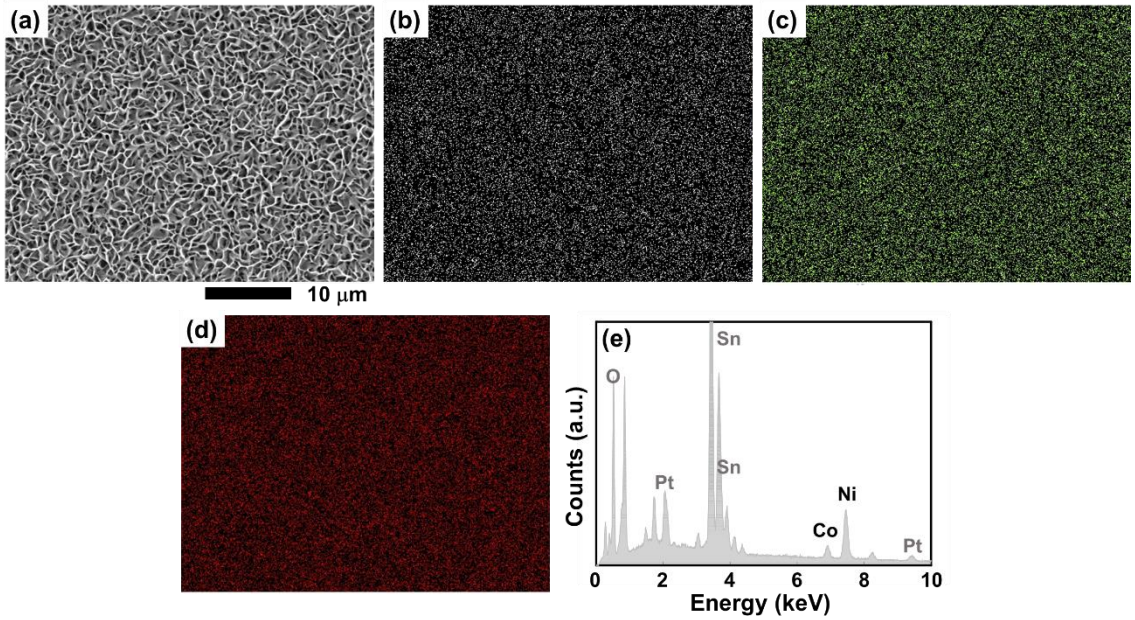

Fig.3.

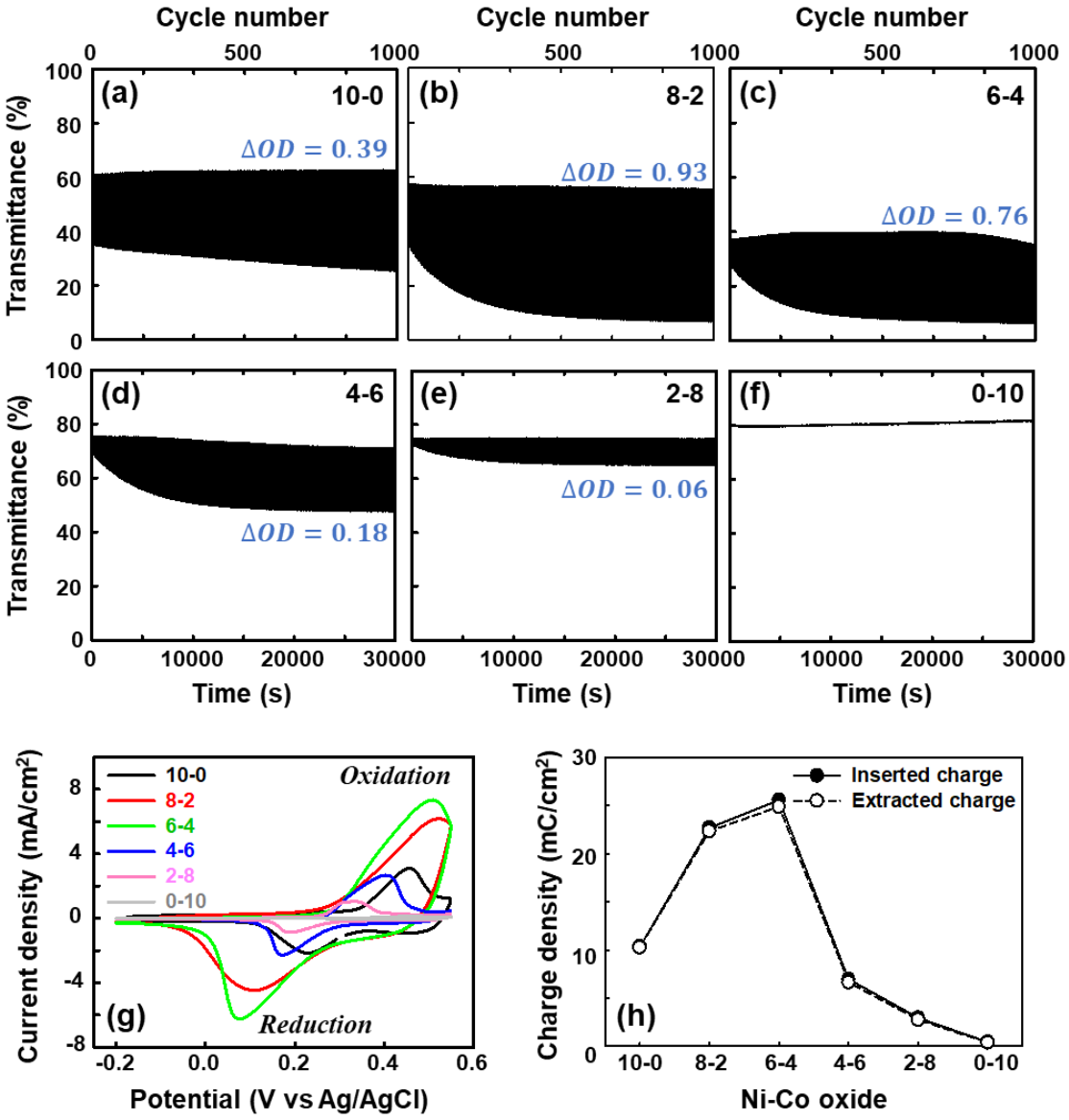
Cycle number
Transmittance (%)
(a)
10-0
ΔOD = 0.39
(b)
8-2
ΔOD = 0.93
(c)
6-4
ΔOD = 0.76
(d)
4-6
ΔOD = 0.18
(e)
2-8
ΔOD = 0.06
(f)
0-10
Time (s)
Current density (mA/cm²)
Oxidation
Reduction
(g)
Potential (V vs Ag/AgCl)
Charge density (mC/cm²)
Inserted charge
Extracted charge
(h)
Ni-Co oxide

Fig.4.

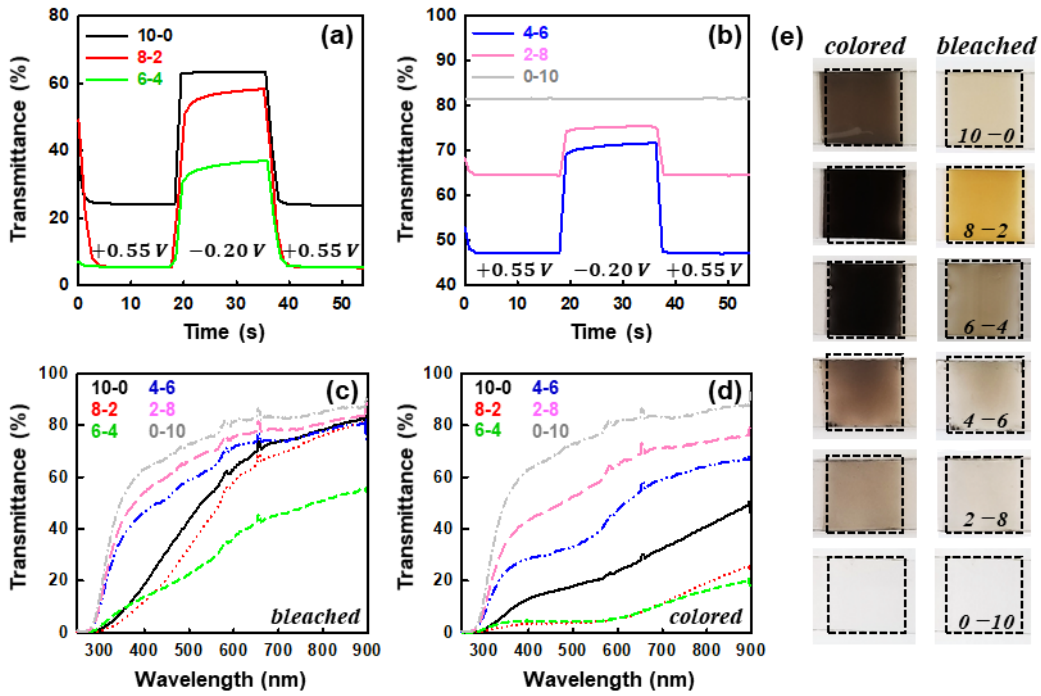
(a)
10-0
8-2
6-4
+0.55 V
−0.20 V
+0.55 V
Transmittance (%)
Time (s)
(b)
4-6
2-8
0-10
+0.55 V
−0.20 V
+0.55 V
Transmittance (%)
Time (s)
(c)
10-0
8-2
6-4
4-6
2-8
0-10
bleached
Transmittance (%)
Wavelength (nm)
(d)
10-0
8-2
6-4
4-6
2-8
0-10
colored
Transmittance (%)
Wavelength (nm)
(e)
colored
bleached
10 −0
8 −2
6 −4
4 −6
2 −8
0 −10

Fig.5.

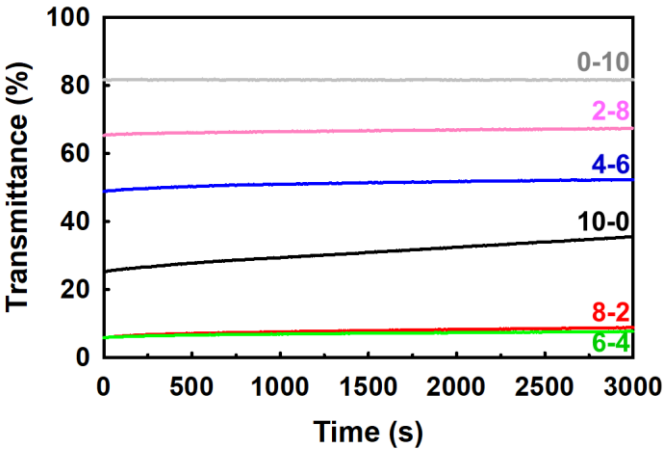
Transmittance (%)
Time (s)
0
20
40
60
80
100
0
500
1000
1500
2000
2500
3000
0-10
2-8
4-6
10-0
8-2
6-4

Fig.6.

Supplementary information

Color modulation of electrochromic nanosheet-structured nickel-cobalt oxide thin films

Kyung Ho Kim*, Misaki Morohoshi, Yoshio Abe

School of Earth, Energy and Environmental Engineering,

Kitami Institute of Technology, 165 Koen-cho, Kitami, Hokkaido 090-8507, Japan

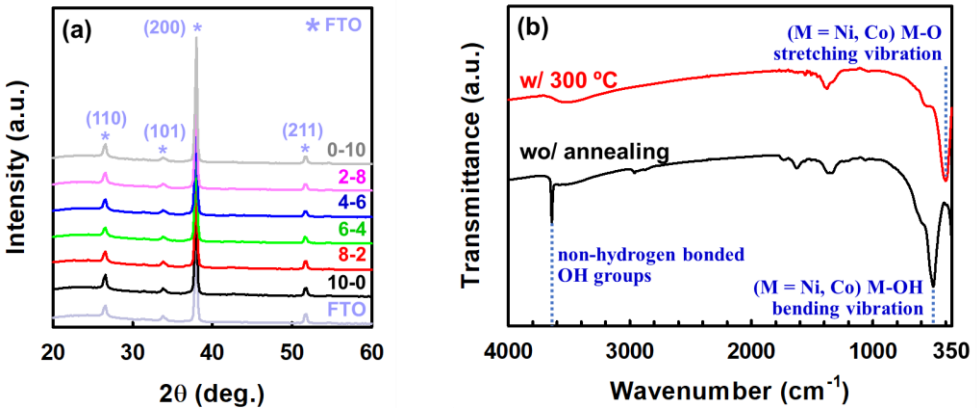

Fig.S1. XRD patterns (a) of Ni-Co thin film samples annealed at 300 ºC and FTIR spectra (b) of Ni8-Co2 powder sample with annealing treatment; Growth time was 6 h.

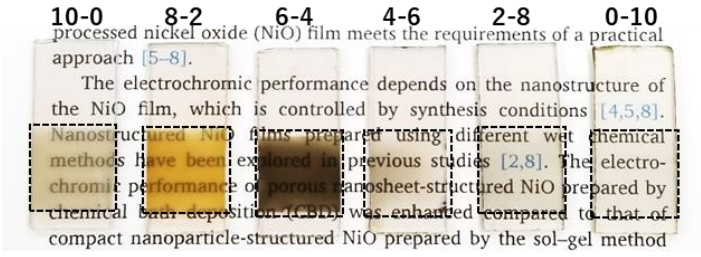

Fig.S2. Photographs of Ni-Co oxide thin film samples directly prepared on FTO/glass substrates; Thin film area was 1 x 1 cm^2; Dotted lines were guide for eye; Growth time was 6 h.

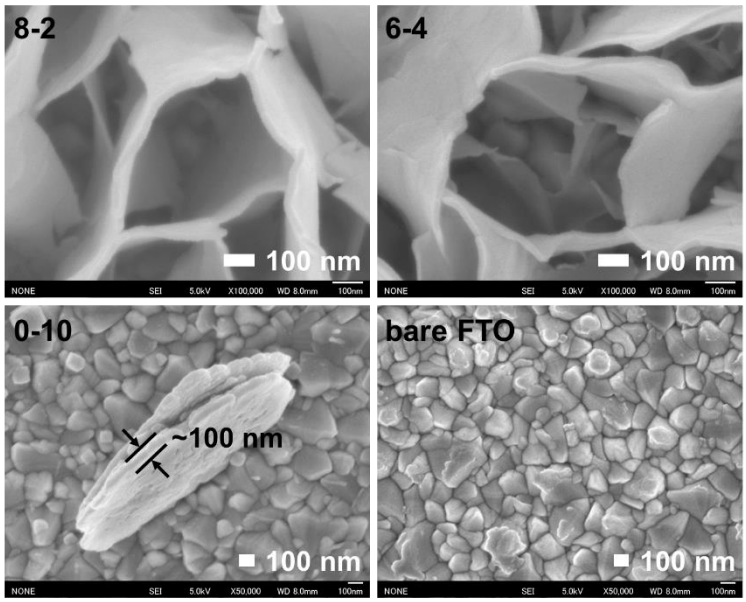

Fig.S3. FESEM images of Ni-Co oxide samples grown for 6 h and bare FTO.

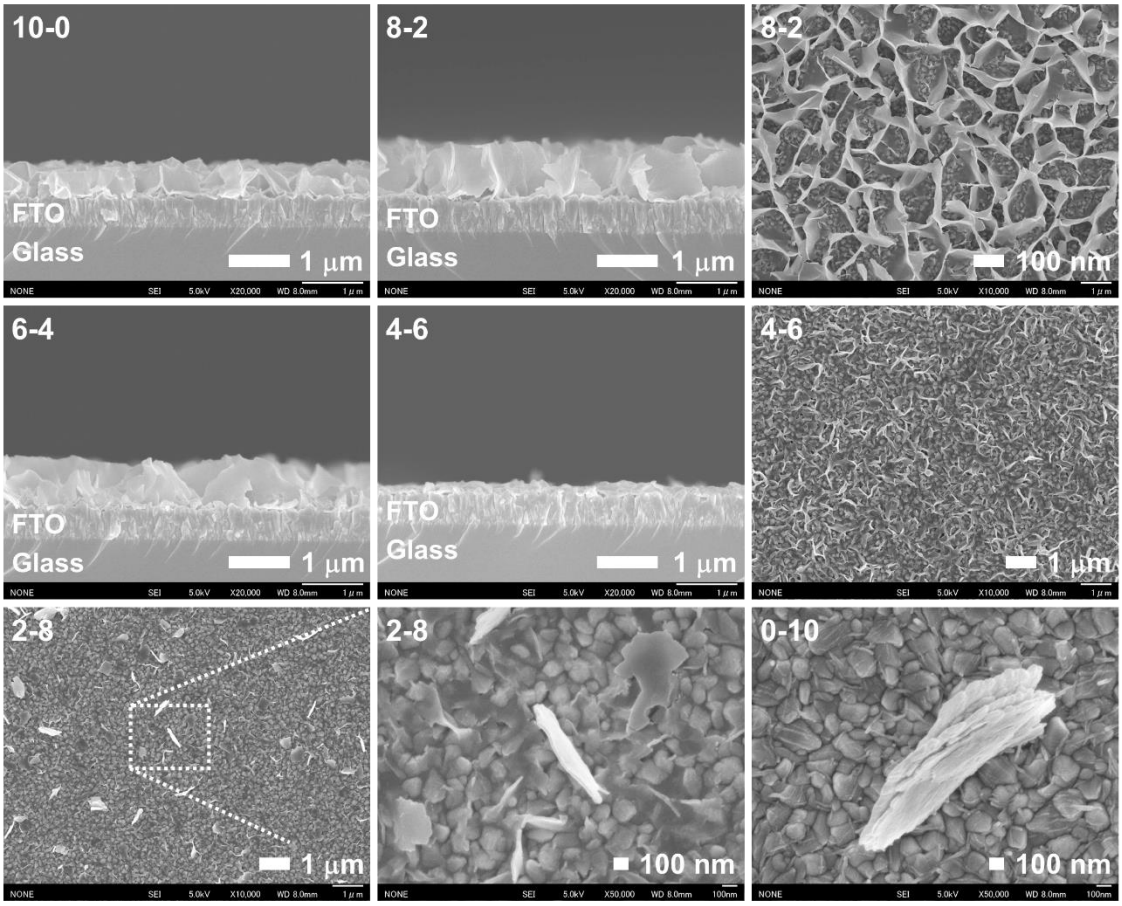

Fig.S4. FESEM images of Ni-Co oxide samples grown for 1.5 h.

Table S1. Ni, Co, and O amounts determined by EDS measurements.

	Ni (wt% / at%)	Co (wt% / at%)	O (wt% / at%)
Ni10-Co0	64.1 / 32.7	–	35.9 / 67.3
Ni8-Co2	49.5 / 23.8	10.1 / 4.9	40.4 / 71.3
Ni6-Co4	39.4 / 18.3	17.4 / 8.1	43.2 / 73.6
Ni4-Co6	23.2 / 9.1	18.0 / 7.0	58.8 / 83.9
Ni2-Co8	11.6 / 4.6	31.6 /12.6	56.8 / 82.8
Ni0-Co10	–	65.7 / 34.2	34.3 / 65.8

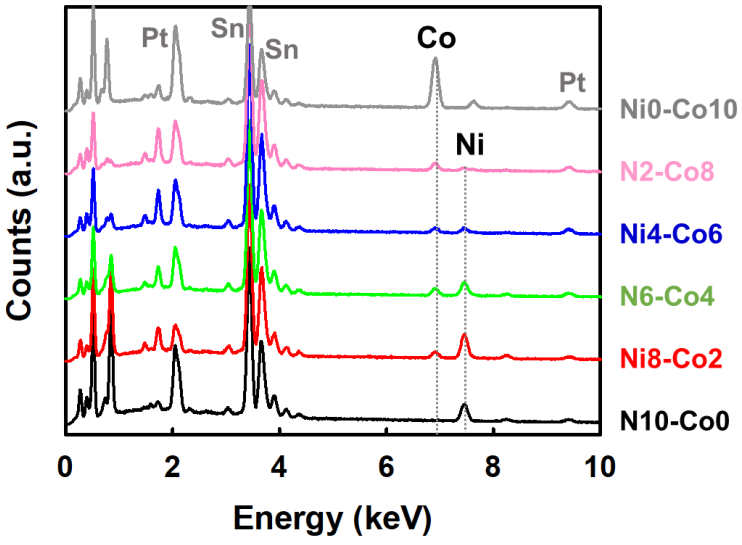

Fig.S5. EDS spectra of Ni-Co oxide samples.

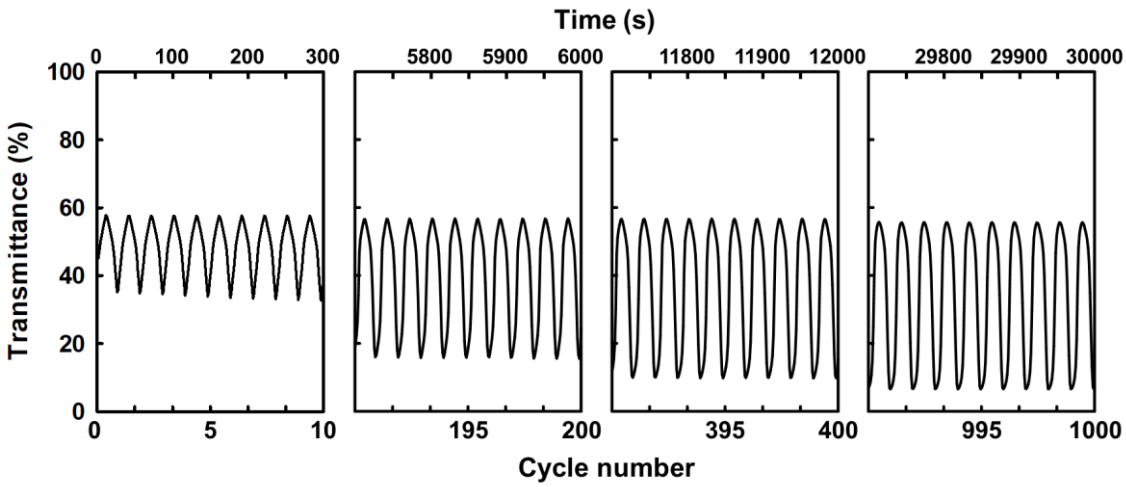

Fig.S6. The *in-situ* transmittance variation of Ni8-Co2 oxide sample during CV cycling.

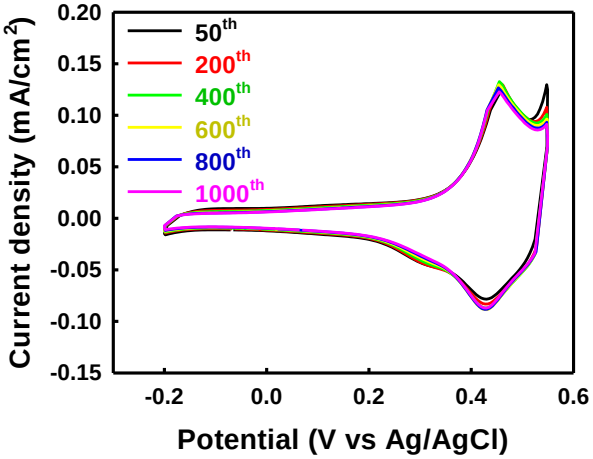

Fig.S7. CV curves of Ni0-Co10 oxide sample at a scan rate of 50 mV/s for 1000 cycles.

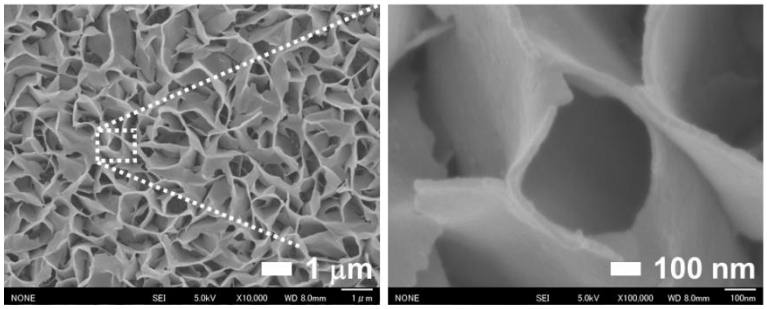

Fig.S8. FESEM images of Ni8-Co2 oxide sample after electrochromic cycling test.

Optical density (ΔOD) [R1]

$$\Delta OD = log \frac{T_{bleached}}{T_{colored}}$$

Color efficiency (CE) [R1]

$$CE = \frac{\Delta OD}{Q_{inserted}}$$

Optical switching time [R1]

: time to reach 90% of the full change in transmittance

[R1] S, Hou, A.I. Gavriluk, J. Zhao, H. Geng, N. Li, C. Hua, K. Zhang, Y. Li, Appl. Surf. Sci. 451 (2018) 104-111.